NANO · MICRO small
www.small-journal.com

Check for updates

Direct Transition from Ultrathin Orthorhombic Dinickel Silicides to Epitaxial Nickel Disilicide Revealed by In Situ Synthesis and Analysis

Philipp M. Wolf, Eduardo Pitthan, Zhen Zhang, Christian Lavoie, Tuan T. Tran, and Daniel Primetzhofer*

Understanding phase transitions of ultrathin metal silicides is crucial for the development of nanoscale silicon devices. Here, the phase transition of ultrathin (3.6 nm) Ni silicides on Si(100) substrates is investigated using an in situ synthesis and characterization approach, supplemented with ex situ transmission electron microscopy and nano-beam electron diffraction. First, an ultrathin epitaxial layer and ordered structures at the interface are observed upon room-temperature deposition. At 290 °C, this structure is followed by formation of an orthorhombic δ-Ni_2Si phase exhibiting long-range order and extending to the whole film thickness. An unprecedented direct transition from this δ-Ni_2Si phase to the final $NiSi_{2-x}$ phase is observed at 290 °C, skipping the intermediate monosilicide phase. Additionally, the $NiSi_{2-x}$ phase is found epitaxial on the substrate. This transition process substantially differs from observations for thicker films. Furthermore, considering previous studies, the long-range ordered orthorhombic δ-Ni_2Si phase is suggested to occur regardless of the initial Ni thickness. The thickness of this ordered δ-Ni_2Si layer is, however, limited due to the competition of different orientations of the δ-Ni_2Si crystal. Whether the formed δ-Ni_2Si layer consumes all deposited nickel is expected to determine whether the monosilicide phase appears before the transition to the final $NiSi_{2-x}$ phase.

1. Introduction

The contact layers between electronic devices and interconnects play a decisive role in the performance and the reliability of integrated circuits. These contacts should provide a low resistant pathway for the electrical current, as well as a diffusion barrier for the interconnects. In the era of extremely scaled silicon complementary metal-oxide-semiconductor (CMOS) devices[1] and devices using nanomaterials, such as 2D materials[2,3] and nanowires,[4,5] there is high demand for understanding the behavior of the contact materials, such as the formation processes and the characteristics of the interface, at length scales of a few nanometers. The behavior of the ultrathin films could substantially deviate from those of the thicker films, due to the much-enhanced influence of the interface.

Reports have shown that under heat treatment a nickel (Ni) film deposited on a silicon (Si) substrate will undergo a transition from Ni-on-Si → orthorhombic δ-Ni_2Si (≈250 °C) → orthorhombic NiSi (≈350 °C) → cubic $NiSi_2$ (≈800 °C).[6–8] However, when the thickness of the initial Ni film is reduced to a critical thickness of less than 4 nm, the transition behavior of the film is found to be substantially different. The as-deposited film quickly transforms to the final $NiSi_{2-x}$ phase at a temperature as low as 320 °C. Furthermore, the formed $NiSi_{2-x}$ phase is epitaxial on the Si substrate which remains stable against further annealing.[9–12] However, due to the challenges in characterizing film composition and structure at nanometer scale, accurate understanding of the phase transition pathways of ultrathin silicides has not been fully established. Using in situ transmission electron microscopy (TEM) in plane view, Gibson et al. have shown the existence of the metastable hexagonal θ-Ni_2Si phase in the silicide films formed out of Ni films with thicknesses less than 2 nm grown on Si(111) substrates. The hexagonal θ-Ni_2Si was found to correlate to the subsequent growth of a type-A $NiSi_2$ at 450 °C.[13] Coming to the same conclusion, Bennett et al. showed that the phase leading to the final $NiSi_2$ phase on a Si(111) substrate is the hexagonal θ-Ni_2Si.[14] Furthermore, their data using surface X-ray diffraction suggested that the first few monolayers of the silicide are epitaxial to the substrate.

P. M. Wolf, E. Pitthan, T. T. Tran, D. Primetzhofer
Department of Physics and Astronomy
Ångström Laboratory
Uppsala University
Box 516, Uppsala SE-751 20, Sweden
E-mail: philipp.wolf@physics.uu.se

Z. Zhang
Solid State Electronics
Department of Electrical Engineering
The Ångström Laboratory
Uppsala University
Uppsala SE-751 21, Sweden

C. Lavoie
IBM Thomas J. Watson Research Center
Yorktown Heights, New York 10598, USA

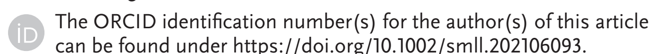
The ORCID identification number(s) for the author(s) of this article can be found under https://doi.org/10.1002/smll.202106093.

© 2022 The Authors. Small published by Wiley-VCH GmbH. This is an open access article under the terms of the Creative Commons Attribution License, which permits use, distribution and reproduction in any medium, provided the original work is properly cited.

DOI: 10.1002/smll.202106093

According to Gibson's study, for thin Ni films the θ-Ni_2Si phase has, however, never been found on a Si(100) substrate. For the Si(100) substrate, using a combination of several electron microscopy and X-ray diffraction techniques, De Keyser et al. suggested that no epitaxy of a single phase can explain all the data.[15] They stated that the ultrathin silicide formed from 3.7 nm Ni at 350 °C is not purely epitaxial, but consists of nanometer domains that share the alignment of a series of atomic planes. Note that in their study further annealing of the film to 600 °C led to the formation of grains of both hexagonal θ-nickel silicide and $NiSi_2$ phases.

Recently, using in situ 3D ion scattering for composition analysis we could distinguish three separate stages of the phase transition of a 3 nm Ni film on a Si(100) substrate, by annealing the film in steps of 30 °C up to 540 °C: as-deposited to 165, 230–290, and beyond 320 °C.[12] The intermediate stage (230–290 °C) with integral composition close to the monosilicide phase is unprecedented, which immediately prompts the interest in understanding this stage thoroughly. This observation may provide key evidence for several long-standing questions in this topic, such as: what is the transition sequence of the ultrathin film? And what is the reason for the strong dependence of the phase transition on the initial Ni thickness? While this intermediate stage was shown to be the immediate precursor phase for the final epi-$NiSi_{2-x}$ phase, no structural characterization has been conducted to verify its phase.[12] For this reason, in the present study we capture the exact moment when the precursor phase starts to transform to the final epitaxial phase, by in situ deposition and controlled annealing of the film to the earlier observed critical temperature of 290 °C. We employed an in situ approach for both growth and characterization using Auger electron spectroscopy (AES), low-energy electron diffraction (LEED), and low-energy ion scattering (LEIS) to study the film after the deposition steps and after annealing. Complementarily, ex situ characterizations using medium-energy ion scattering (MEIS), high-resolution TEM (HR-TEM), and electron diffraction with a nanoscale probe were employed to study the film's composition, the crystal structure of the precursor phase, and the characteristics of the interface. We used the combination of these in situ and ex situ techniques to obtain sufficient information for better understanding of the transition process of the ultrathin Ni silicide, and hence to provide a plausible explanation for the dependence of the transition on the initial Ni thickness.

2. Results

2.1. In Situ Growth and Characterization

Figure 1 shows the AES spectra of the sample at the sequential stages of the experiment, such as the Si substrate after sputter cleaning, the Ni film after deposition, and the Ni film after annealing at 290 °C. Since the Auger electrons have sub-keV energies, and hence a short inelastic mean free path, the AES spectra are highly surface sensitive and contain information on the sample composition within the top few monolayers from the surface.[16] As shown in Figure 1a, the spectrum after several cycles of sputtering and annealing includes only the Si peak indicating a surface free from contaminants, such as carbon and oxygen. Additional AES spectra were also recorded during

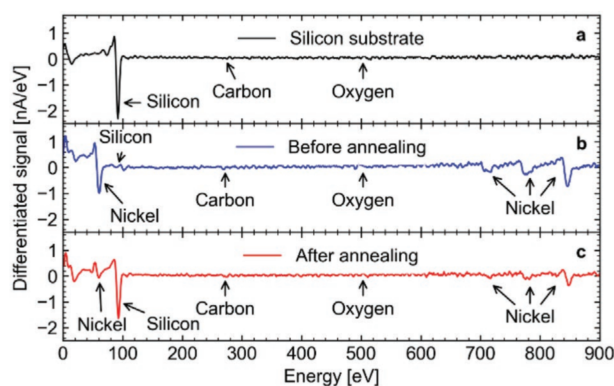

Figure 1. The AES spectra obtained using 3 keV primary electrons: a) after sputter cleaning, b) after deposition of Ni for 32 min, and c) after annealing at 290 °C. Spectrum (a), belonging to the Si substrate, shows no visible oxygen, carbon, or other surface impurities. After deposition, spectrum (b) shows clear Ni peaks at energies of 61, 716, 783, and 848 eV, while the Si peak at 92 eV is minor. After annealing (c) the size of the Ni peaks is reduced while the Si peak at 92 eV significantly increases in size.

the Ni deposition process after 8, 16, and 32 min (Figure S1, Supporting Information). The oxygen or carbon peaks are visible in neither of those spectra, signaling a Ni layer free from contaminants. For the large part of the total deposition duration of 32 min, the Si peaks and the Ni peaks both appeared in the spectra, indicating either an island growth of the Ni layer, or the intermixing of Ni and Si within the same layer. Intermixing effects, even for deposition at room temperature, have been reported several times in literature for both e^--beam and sputter deposition.[9,12,17,18]

After deposition for 32 min the topmost layer of the film is found to comprise of mainly Ni as virtually only the Ni peaks can be seen in the final spectrum of Figure 1b. After annealing at 290 °C, the Si peak appeared strongly again as shown in Figure 1c, indicating a reaction between the Ni and the Si, increasing the Si fraction within the surface layer. Calculations of the surface composition based on the peak-to-peak heights result in 6% Si to 94% Ni before annealing and 68% Si to 32% Ni after annealing. No evidence for significant contamination is visible in the spectra at any stage of the process (the expected positions of the O-signal and the C-signal are indicated). The LEED images obtained after cleaning the substrate and after annealing the sample are included as supplements (Figure S2, Supporting Information). The LEED image recorded after substrate cleaning shows a clear 2 × 1 surface reconstruction of the Si substrate. After annealing of the Ni silicide, the surface shows a quadratic diffraction pattern in the LEED image, indicating a highly ordered tetragonal surface structure. Prior to annealing no pattern was observable in LEED, indicating the absence of any long-range order on the sample surface.

Figure 2a includes the time-of-flight low-energy ion scattering (ToF-LEIS) spectra recorded for the Si substrate, the sample before annealing and the sample after annealing. In the spectra of the Si substrate clear effects stemming from the crystallinity of the sample are visible, like a distinct surface peak[19] and an increase of counts toward lower energies. After Ni deposition but before annealing a pronounced Ni peak is visible, overlapping with the signal due to silicon. Indications for an intermixing layer of Ni and Si are again found in the

© 2022 The Authors. Small published by Wiley-VCH GmbH

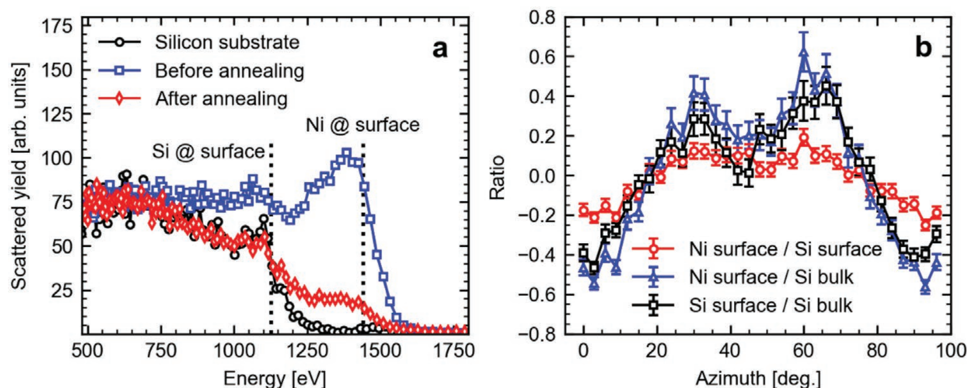

Figure 2. a) The energy spectra of 1.8 keV He^+ ions scattered from the sample surface, prior to Ni deposition (black curve), after Ni deposition (blue curve), and after annealing to 290 °C (red curve). The kinematic edges of He scattered from Si at 1127.6 eV and Ni at 1440.8 eV are included as vertical lines. After annealing the Ni peak height is significantly reduced. b) Ratios between counts in three different areas of the same size in the ToF-LEIS spectra recorded during an angular scan along the azimuth angle at a polar angle of 0° with 1.8 keV He^+ ions. The average of the ratios is shifted to zero for better comparability. The ratio between the Ni peak and the Si peak areas is most stable, while the ratios including the Si bulk area are almost the same indicating a crystalline Ni silicide layer.

ToF-LEIS spectra recorded at different stages of the Ni deposition process (Figure S3, Supporting Information). During the Ni growth a clear signal potentially corresponding to Si atoms on the sample surface, at the same kinematic energy of 1127 eV, is observed at least up to a deposition time of 16 min. Annealing the sample at 290 °C changes the ToF-LEIS spectrum significantly, with the Ni peak being reduced to roughly a fourth of its original height. This prominent signal reduction in combination with the Si edge returning to its pre-deposition state, cannot be explained only by the formation of a silicide phase, but requires a well-ordered structure of the resulting layer. Further analysis of this structure can be performed on the basis of recorded angular scans. Figure 2b shows the ratios of the scattering yield in different areas of the ToF spectra recorded at azimuth angles between 0° and 96°, for normal incidence. Note that averages were shifted to zero for easier comparison. The ratio between the Ni and the Si surface signal is found to be the most stable. The ratios between the surface signals for both Ni and Si and the Si bulk show a stronger angular dependence and are found to be very similar. They show distinct minima at 3° and 87° and a minor minimum around 45°, while having maxima at approximately 30° and 60°. This clear angular dependence of the ratios is not only visible in the azimuth scan, but similarly in the polar scan recorded at an azimuth angle of 0° (Figure S4, Supporting Information). The angular dependence of all shown ratios is an indication for a well-ordered crystalline structure of the thin film which potentially could be fully epitaxial. The similarity between the peak to Si bulk ratios for both Ni and Si agrees with expectations for a film being composed of a mixture of Ni and Si, which is further corroborated by the comparably high stability of the ratio of the surface signals. The fact that, while being more stable than the surface to bulk signals, the Ni peak to Si peak ratio is showing an angular dependence is an indication for a difference in the crystal structures between the Ni silicide and the Si substrate. The fourfold symmetry indicated by the polar scan presented in Figure 2b, however, is an indicator for a cubic or tetragonal structure primarily compatible with the disilicide phase. This phase, nonetheless, is not expected to be formed at the present temperature.[12] These indications, questioning the expected structure of the annealed film, motivate further characterization of the crystalline Ni silicide layer using ex situ measurements to define the exact structure of the film.

2.2. Ex Situ Characterization

As the overlap between the Ni and the Si signals in the ToF-LEIS spectra makes it difficult to quantify the composition of the ultrathin film annealed at 290 °C, we also performed an ex situ ion scattering measurement at a higher primary energy using a ToF-MEIS setup. We chose the primary energy of the He ions to be at 50 keV because at this energy the interaction between the ions and the sample can still be reasonably well described by single scattering, and hence is more quantifiable than the ToF-LEIS for identifying the film's composition. At the same time, the depth resolution is sufficient to clearly resolve the film with a thickness of a few nanometers. As shown in **Figure 3**, the Ni peak is well separated from the Si signal with a visible plateau.

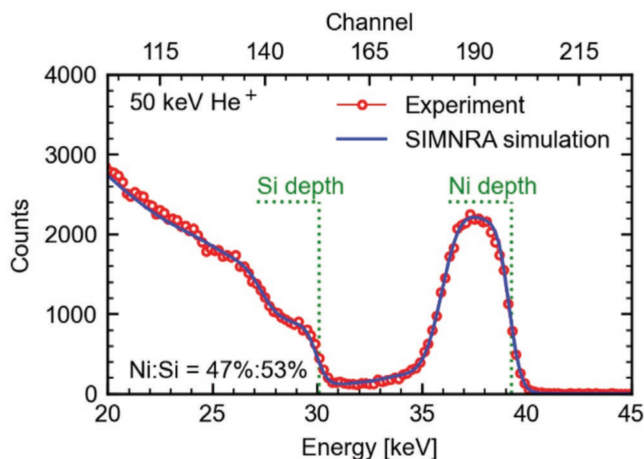

Figure 3. ToF-MEIS data of the film annealed at 290 °C (red circle). Simulation using SIMNRA (blue line) shows the film consists of 47% Ni and 53% Si.

© 2022 The Authors. Small published by Wiley-VCH GmbH

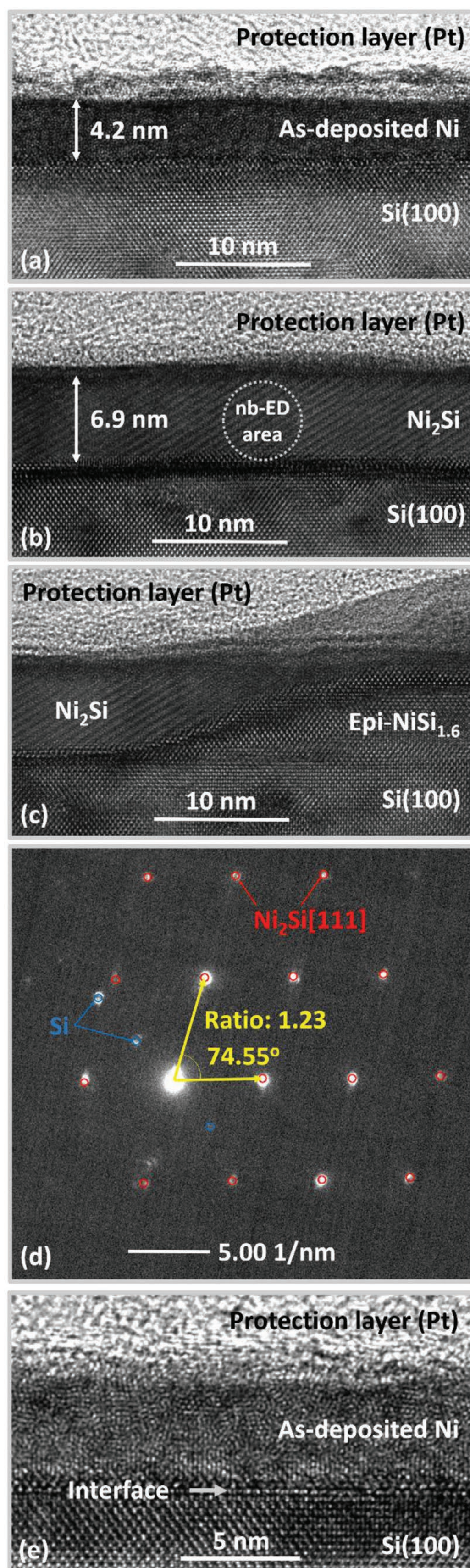

Simulation of the scattering spectrum using SIMNRA and the experimental energy loss extracted from ref. [20] indicates that the composition of the film is 53% Si and 47% Ni, close to the 1:1 ratio of the monosilicide phase. In terms of the composition, this ratio is consistent with the intermediate stage reported in ref. [12] for a similar film annealed at the same temperature of 290 °C. Investigating this stage, between the Ni_2Si and the $NiSi_2$ phase in the transition sequence of an ultrathin Ni silicide may yield key information for understanding the peculiar transition exhibited by ultrathin films toward an epitaxial phase at relatively low temperature. The ToF-LEIS and LEED analysis presented above, however, indicate a cubic or tetragonal structure is present, which is not in accordance with expectations for a trivial monosilicide phase. For that purpose, in addition to the compositional characterization, we performed ex situ structural analysis of this middle stage using HR-TEM and nano beam-electron diffraction (nb-ED) as shown in **Figure 4**.

According to our thickness measurement using Rutherford backscattering spectrometry (RBS), the thickness of the Ni film after deposition is expected to be 3.6 nm, assuming the film is pure Ni with the bulk density of 8.9 g cm^{-3}. Based on the HR-TEM image of the film (Figure 4a) from a twin sample that was not annealed after deposition, its thickness is ≈4.2 nm, slightly higher than the RBS data. This difference might be due to the intermixing between Ni and Si, due to room-temperature reactions as mentioned previously. Another possible contribution to the difference in observed thickness between the RBS and the TEM is that the thin film is expected to feature lower density than the bulk value. Structurally, this layer is close to an amorphous phase as no atomic order can be observed in the present HR-TEM image. After annealing at 290 °C, the film characteristics have changed as shown in Figure 4b,c. First, the thickness of the film increased from ≈4.2 to ≈6.9 nm due to the reaction of the deposited film with the Si substrate. Second, atomic ordering of the structure can be observed, such as the periodic diagonal streaks in Figure 4b that occupy a large volume of the film, indicating a single-crystal phase, which is in registry but not epitaxial to the substrate, being rotated off axis to the [100] zone axis of the Si substrate. The residual more minor fraction of the film is occupied by the epitaxial phase to the right in Figure 4c, which we assign to the non-stoichiometric $NiSi_{2-x}$ as reported in ref. [12]. Figure 4c apparently shows that we have captured the exact moment when the film started to transform to the epitaxial $NiSi_{2-x}$ phase from its precursor, the diagonal-streak phase, with the transition occurring at a 2d boundary between the two phases. Hence, information about the phase of the diagonal-streak region will significantly improve our understanding on the unique phase transition of the ultrathin Ni silicide. Indications on the nature of the ultrathin Ni silicide can be obtained from the mass density of some common Ni silicide phases, such as the Ni_2Si (d = 7.35 g cm^{-3}) and the NiSi (d = 5.93 g cm^{-3}), based on

Figure 4. HR-TEM micrographs of the a) as-deposited and b,c) the as-annealed sample. Figure (b) shows the area where the Ni_2Si phase is dominant, whereas there is a mix of the Ni_2Si and the epi-$NiSi_{2-x}$ phase in Figure (c). d) The electron diffraction pattern from the area circled in Figure (b). e) A magnified HR-TEM image of the as-deposited film, showing the well-ordered structure of the film at the interface.

© 2022 The Authors. Small published by Wiley-VCH GmbH

which we can calculate the expected thickness of the film, if it is one of these phases, from the initial Ni film of 3.6 nm. If the diagonal phase is NiSi, the expected thickness would be ≈8 nm. Otherwise, if it is the Ni_2Si phase, its thickness would be 5.4 nm. Because the film thickness as measured from Figure 4b is 6.9 nm, we think the latter case would be more likely since the surplus of the calculated NiSi thickness (8 nm) compared to the measured thickness of the layer could only be explained by an increased mass density which is unlikely. The thickness deficit in the latter case of Ni_2Si (5.4 nm), as compared to the measured thickness, can be compensated by a reduced mass density of the Ni_2Si film due to vacancy defects. Another possible explanation for the film thickness is that the film consists of a mixture between denser Ni_2Si and less dense epi-$NiSi_{2-x}$ or NiSi. While indicating the existence of Ni_2Si in the film, these thickness considerations do not yield a conclusive answer to the nature of the films phase.

To gain more information about the crystal structure of the diagonal streaks, we have performed nano-beam electron diffraction at the area marked by the dot circle in Figure 4b. In order to find a zone axis of the film, we had to rotate the sample about 5° along the [100] zone axis of the substrate. Figure 4d presents the diffraction pattern of the film (the red-circle pattern), together with some diffraction spots from the substrate or the epi-$NiSi_{2-x}$ regions that have the same crystal structure as the substrate (the blue circles). Based on this diffraction pattern, we have used an electron microscopy simulation software, JEMS, to find a matching pattern from all known Ni silicide phases. It was indicated that the best fitting pattern for the measurement is the diffraction pattern from the Ni_2Si phase, obtained when the electron beam is aligned with the [111] zone axis of the phase. As measured from Figure 4d, the angle between the two yellow arrows pointing from the origin to the two closest reflections (spot order 1) is 74.55°, and the length ratio between them is 1.23. These numbers are very close to the theoretical values for the pattern of the δ-Ni_2Si[111], which are 74.392° and 1.24, respectively. Although the NiSi phase has the same orthorhombic structure and the same space group Pnma as the δ-Ni_2Si, the angle and the length ratio for the NiSi[111] is 69.7° and 1.33, respectively, considerably different from the measured values. Note, that we found no evidence for the formation of the θ-phase at the present temperature.

Hence, our conclusion is that in the phase transition of the ultrathin Ni silicide film the film transforms directly from the orthorhombic δ-Ni_2Si structure to the non-stoichiometric epitaxial cubic $NiSi_{2-x}$ structure, completely skipping the intermediate monosilicide NiSi phase. In terms of composition, the film annealed at 290 °C has a composition close to the monosilicide phase, also consistent with our previous study[12] and results by De Keyser et al. obtained at slightly higher temperature of 350 °C.[15] However, based on the new diffraction data the 1:1 composition can be explained by the film being a mixture of the Ni-rich δ-Ni_2Si and the Si-rich $NiSi_{2-x}$, that in combination makes up the equal content of Ni and Si, different from the phase being nickel monosilicide structurally. The existence of the epitaxial cubic $NiSi_{2-x}$, which is confirmed by Figure 4c, also explains the atomic ordering as found from the angular scan ToF-LEIS data (Figure 2b) and the tetragonal pattern of the LEED data (Figure S2, Supporting Information). In Figure S5 (Supporting Information), we show a series of diffraction patterns taken along the film. In all of these patterns, the δ-Ni_2Si[111] appears predominantly in almost all the figures, further affirming the decisive role of this phase in the transition to the final epitaxial phase.

Before going further into the discussion, we show a different HR-TEM image of the as-deposited film (Figure 4e), similar to Figure 4a, but with higher magnification. At the film/substrate interface, some first few monolayers can be seen as epitaxially grown on the substrate. The epitaxial layer is then covered by another layer of well-ordered vertical lines, extending to up to 40% of the total film thickness at some areas. This data shows that the reaction of Ni and Si did not only occur at room temperature, but also formed a commensurate structure with the substrate.

3. Discussion

In light of our observation of an orthorhombic δ-Ni_2Si phase as the precursor for the epitaxial cubic $NiSi_{2-x}$, and the formation of an ordered structure upon deposition at the interface, we will in the following discuss literature related to the topic and then try to provide an explanation for the dependence of the phase transition on the thickness. Using in situ TEM and diffraction during growth, Gibson et al. have found that the metastable hexagonal θ-Ni_2Si phase occurred at a temperature of 300 °C. This phase correlates with the subsequent growth of the epitaxial $NiSi_2$ at 450 °C on the Si(111) substrate.[13] The existence of the θ-phase with a Si content from 33% (Ni_2Si) to 40% has been always observed in the 10 nm Ni films on Si(100) substrates by Gaudet et al., regardless of dopant, film thickness, deposition method, and anneal conditions (>2000 conditions).[21] However, for the ultrathin Ni film on Si(100) substrates, Gibson et al. have never found this phase.[13]

Another study comparable to ours, which was performed by De Keyser et al. with 3.7 nm Ni on Si(100),[15] showed that there is no single epitaxy of currently known nickel silicides that can explain all the data. Hence, they proposed that the film preceding to the final epi-$NiSi_2$ phase is composed of nano-domains that shared the alignment of atomic planes. According to our result, we indeed found that the film annealed at 290 °C has some different phases, such as the δ-Ni_2Si, the δ-Ni_2Si phase with different orientations (Figure S5, Supporting Information), and the final epi-$NiSi_{2-x}$ which we have resolved in our previous paper as $NiSi_{1.6}$.[12] However, besides the final epi-$NiSi_{2-x}$, the δ-Ni_2Si is the most abundant and the crystal size extends laterally hundreds of nanometers along the film. Therefore, we conclude that the final epitaxial film is induced by the large crystallites of the δ-Ni_2Si phase.

Based on the available information extracted from the past and current works, we propose a pathway for the reactions of the ultrathin Ni silicide as follows. At the early stage, the deposited Ni reacts with Si in a commensurate way to form a few epitaxial monolayers as revealed by Figure 4e. Upon further deposition, the deposited Ni atoms continue to react with the Si substrates as shown by the ToF-LEIS data (Figure 2a) and the AES spectra (in Supporting Information). This data is

© 2022 The Authors. Small published by Wiley-VCH GmbH

supported by a study by Bennett et al. who used surface X-ray diffraction and found the epitaxial nature of the first few monolayers at the interface. Above these epi-monolayers, a non-epitaxial, but "ordered" film with the stoichiometry of Ni_2Si forms up to 3 nm until the reaction dramatically slows down and stops. The deposition of additional Ni then results in an unordered Ni film covering the previously grown structure.[14] Upon annealing up to 290 °C, the partially ordered Ni_2Si film transforms to well-ordered orthorhombic δ-Ni_2Si as shown by the TEM data of Figure 4. The δ-Ni_2Si subsequently transforms directly to the epitaxial cubic $NiSi_{2-x}$ at temperature >290 °C. Under thermodynamic consideration, the δ-Ni_2Si phase would be more favorable to transform to the monosilicide NiSi phase as observed for thicker films, before transforming to the final $NiSi_2$ phase. However, the δ-Ni_2Si phase as shown in this study has a well-ordered structure, extending over the whole layer thickness. The formation of this layer is expected to be made feasible, by the ordered precursor structures making up a significant fraction of the deposited layer. In other words, both after deposition, and also during annealing, a high fraction of the deposited material exhibits an ordered structure heavily influenced by the substrate. In consequence, it can translate the crystal characteristics of the substrates more effectively, that is, creating an enhanced interfacial effect. This effect effectively dictates the fast and direct reaction process toward the final epitaxial $NiSi_{2-x}$ as a more favorable phase due to its structural similarity with the substrate, instead of going through the monosilicide phase with a dissimilar crystal structure.

We argue that the same formation process occurs in all Ni-on-Si(100) samples. Irrespective of the final nominal thickness of the initially deposited Ni, the first few monolayers of the resulting film will be epitaxial, followed by a partially ordered Ni_2Si layer which then transforms to the well-ordered δ-Ni_2Si phase at elevated temperature. However, the thickness of this well-ordered structure extends only up to a certain thickness, of a few nanometers. This condition is rationalized by the fact, that the resulting Ni_2Si phase, can exhibit a multitude of different orientations, which start to increasingly interact with each other, for thicker films, as the interface area between these crystallites increases relative to the area in registry with the substrate. Thus, at a maximum thickness of the well-ordered dinickel silicide further reaction is hampered. If this reaction has not consumed all deposited Ni, the reaction pathway via the monosilicide is favored upon further annealing. If all Ni is consumed, the high registry with the substrate favors the direct transition to the $NiSi_{2-x}$ phase. Evidence for this argument can be found in one of our previous studies for annealing of a 10 nm Ni film on Si(100), specifically in ref. [22]. In that study, for the 10 nm Ni sample we observed a two-step profile of the film annealed at 225 °C (Figure 1b in ref. [22]), in which the interfacial layer is found to feature a composition in agreement with the Ni_2Si phase and a thickness of ≈9 nm. According to the conversion ratio between the thickness of the δ-Ni_2Si and the thickness of the initial Ni ($t_{\delta\text{-Ni2Si}}/t_{\text{Ni}} = 1.5$), the amount of Ni required for forming the 9 nm δ-Ni_2Si layer is ≈6 nm,[23] which is similar to the Ni thickness often reported for the direct transition to the ultrathin epi-$NiSi_{2-x}$ films.

4. Conclusion

We used in situ growth, annealing, and characterization of ultrathin Ni silicides on a Si(100) substrate. Upon deposition at room temperature, an interfacial reaction between the Ni and the Si is observed as shown by the AES and ToF-LEIS spectra. This reaction leads to the formation of a few epitaxial monolayers at the interface, followed by a well-ordered vertical line structure extending to 30 –40% of the film thickness as revealed by the TEM study. Upon annealing the film to 290 °C, we can deliberately capture the exact transition point of the precursor phase to the final epitaxial $NiSi_{2-x}$ phase. The precursor phase is large crystallites extended through the whole thickness of the films and hundreds of nanometers laterally. Nano-beam electron diffraction within this layer indicated that the precursor crystal is the orthorhombic δ-Ni_2Si, which then transforms directly to the final cubic $NiSi_{2-x}$ at 290 °C, totally skipping the transition pathway via NiSi as the normally occurring phase for the thicker films. We suggest that due to the initial order close to the interface, the δ-Ni_2Si phase can be formed over the whole film thickness which might translate the crystal structure of the interface more efficiently. Thus, the film is more readily transformed to the epitaxial cubic $NiSi_{2-x}$ phase than the monosilicide NiSi which has a different structure than that of the substrate. With evidence from our previous study, we suggest that at the interface to the substrate the ordered δ-Ni_2Si phase is always formed after annealing at 230–290 °C, regardless of the initial Ni thickness. However, the thickness of the ordered δ-Ni_2Si layer is limited to a few nm, due to competition between different orientations, which ultimately determines whether the film will transform to the final epi-$NiSi_{2-x}$ phase for ultrathin films or the NiSi phase for the thicker film samples upon further annealing.

5. Experimental Section

The experiments were conducted in ultra-high vacuum environment of 10^{-10} mbar to be able to prepare an ultra-clean Si surface and to minimize the level of contamination. Such contamination and doping had been shown to considerably affect the phase transition of both ultrathin[24] and thicker films.[25] Prior to the thin film deposition, surface impurities of a p-type Si(100) substrate (Silicon Materials, 10–20 Ω cm) were removed by multiple cycles of ion sputtering with a 3 keV Ar^+ beam and subsequent annealing at ≈800 °C. This cleaning procedure resulted in a contaminant-free Si(100) lattice exhibiting a 2 × 1 surface reconstruction as verified by AES and LEED. Next, the Ni film was deposited in situ on the substrate by electron beam evaporation from a Ni rod. The e-beam evaporator (UHV Evaporator 3T by Omicron) was operated at a filament current of 2.85 A and a high voltage of 1 kV at pressures lower than 5×10^{-10} mbar, which resulted in a nominal deposition rate of 0.105 nm min^{-1}. After a total deposition time of 32 min, a nominal Ni layer thickness of 3.36 nm was expected. Ex situ thickness measurement using RBS with a 2 MeV He^+ beam showed the areal density of the Ni film was 32.5×10^{15} atoms cm^{-2}. Assuming the Ni film had a bulk density of 8.9 g cm^{-3}, the actual thickness of the film therefore would be 3.6 nm. The deposition process was paused two times, first after 8 min and again after 16 min of the total deposition time to perform AES, LEED, and ToF-LEIS measurements to monitor the deposition steps. The AES measurements, performed with a PHI 10-155 AES system at a beam energy of 3 keV, neither detected carbon nor oxygen during any stage of the thin film growth. LEED pictures were obtained utilizing an ErLEED 3000 setup. Additionally, all three measurements were

© 2022 The Authors. Small published by Wiley-VCH GmbH

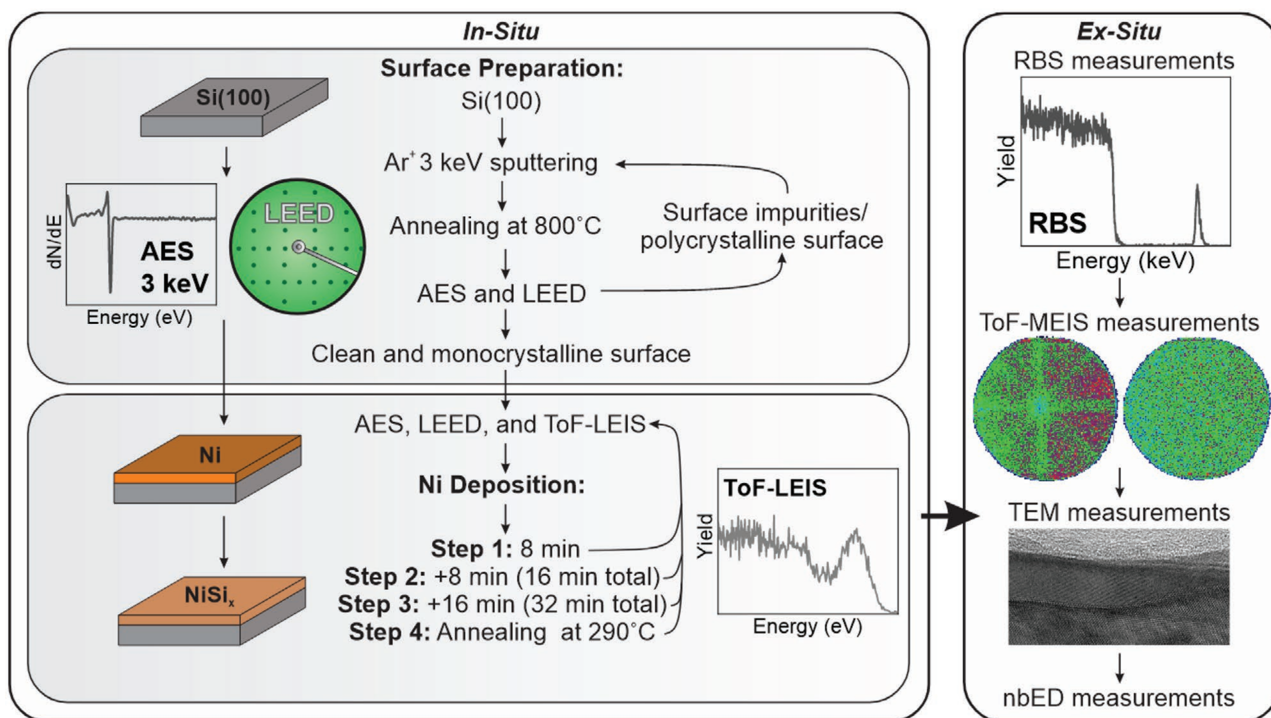

Figure 5. Schematics of the experiment: The Si substrate preparation, the Ni deposition, multiple AES, LEED, and ToF-LEIS measurements were conducted in situ and followed by ex situ RBS, ToF-MEIS, and TEM analyses.

performed after the full 32 min of deposition and after annealing the sample for 10 min at a temperature of 290 °C during which the pressure did not rise above 3.1×10^{-10} mbar. The temperature was indicated by a thermocouple that was in direct contact with the sample surface and calibrated using the melting temperatures of two metals, indium and lead, as references. An additional sample was prepared following the same cleaning process and a single Ni deposition step of 32 min, with neither of the in situ methods detecting a difference between the two samples. This sample was not annealed after deposition to be used for comparison. The ToF-LEIS measurements were performed in situ using a 1.8 keV He^+ beam in the ACOLISSA setup[26] with a scattering angle of 129°, a detector acceptance angle of 0.29°, an incident angle of 0°, and an exit angle of 51°, both with respect to the surface normal. ToF-LEIS can be classified as a non-destructive method due to the low primary ion currents, for the present experiment, amounting to roughly 2.5×10^{10} ions per mm^2 during a typical measurement time of 600 s with a beam spot size of 2.25 mm^2, which was significantly lower than the roughly 10^{13} surface atoms per mm^2, so that the introduced lattice disorder was insignificant. An overview of the sample preparation and measurements is illustrated in Figure 5.

Further information on the crystalline structure of ultrathin films was obtained by performing angular scans in ToF-LEIS.[27,28] Both azimuthal scans, rotating the sample around the surface normal, and polar scans, rotating the sample around the normal of the beam-detector-plane, were performed. In our setup the polar angle was defined as the negative of the incident angle. Uncertainties included in the plotted ratios between different spectrum areas are statistical errors originating from the number of counts in the individual areas.

In addition to the described in situ experiments, complementary ex situ characterizations were performed. They included ToF-MEIS, HR-TEM, and nb-ED. The ToF-MEIS was performed using the 3D ToF-MEIS system at Uppsala University[29,30] with a 50 keV He^+ beam, a scattering angle of 140°, an incident angle of 15°, and an exit angle of 25°, the latter again with respect to the surface normal. As compared to conventional RBS, MEIS provided improved depth resolution, and was thus more suitable for determining the composition of ultrathin films.[31] The acquired ToF-MEIS spectrum was then analyzed using the SIMNRA simulation program[32] with a modified stopping power obtained experimentally for this energy.[20] Regarding electron microscopy, TEM lamellae were extracted from the sample using focused ion beam (FEI DualBeam FIB/SEM235) and in situ lift-out. The nickel silicide layer was protected during the application of the focused ion beam by a protective Pt layer. Due to the TEM analysis being the last experiment performed on the sample, the Pt layer was not present for all prior measurements and the annealing. TEM analysis was conducted with a FEI Titan Themis 200 system at an acceleration voltage of 200 kV. The performed methods include HR-TEM for imaging the as-grown and the as-annealed films, and the nb-ED for structural determination of the film after being annealed at 290 °C. The diffraction patterns were evaluated using JEMS, a simulation software that allows the comparison between the recorded pattern and simulated patterns generated from known crystal structures.

Supporting Information

Supporting Information is available from the Wiley Online Library or from the author.

Acknowledgements

Support by the Swedish Research Council VR (contracts #2016-03432 & #2020-04754) is gratefully acknowledged. Support of the accelerator operation at Uppsala University by VR-RFI (contracts #2017-00646_9 and #2019-00191) and the Swedish Foundation for Strategic Research (SSF, contract RIF14-0053) is gratefully acknowledged. Z.Z. acknowledges a grant from the Swedish Foundation for Strategic Research (SSF, contract No. SE13-0333).

© 2022 The Authors. Small published by Wiley-VCH GmbH

Conflict of Interest

The authors declare no conflict of interest.

Data Availability Statement

The data that support the findings of this study are available from the corresponding author upon reasonable request.

Keywords

epitaxial silicide, in situ characterization, ion scattering, nickel silicide, ultrathin metal silicides

Received: October 7, 2021
Revised: December 22, 2021
Published online: February 21, 2022

[1] Z. Zhang, S.-L. Zhang, B. Yang, Y. Zhu, S. M. Rossnagel, S. Gaudet, A. J. Kellock, J. Jordan-Sweet, C. Lavoie, *Appl. Phys. Lett.* **2010**, *96*, 071915.
[2] L. Wang, I. Meric, P. Y. Huang, Q. Gao, Y. Gao, H. Tran, T. Taniguchi, K. Watanabe, L. M. Campos, D. A. Muller, J. Guo, P. Kim, J. Hone, K. L. Shepard, C. R. Dean, *Science* **2013**, *342*, 614.
[3] D. S. Schulman, A. J. Arnold, S. Das, *Chem. Soc. Rev.* **2018**, *47*, 3037.
[4] Y.-C. Lin, Y. Chen, Y. Huang, *Nanoscale* **2012**, *4*, 1412.
[5] Y.-C. Chou, W.-W. Wu, L.-J. Chen, K.-N. Tu, *Nano Lett.* **2009**, *9*, 2337.
[6] C. Lavoie, F. M. d'Heurle, C. Detavernier, C. Cabral, *Microelectron. Eng.* **2003**, *70*, 144.
[7] F. M. d'Heurle, P. Gas, *J. Mater. Res.* **1986**, *1*, 205.
[8] S. Gaudet, P. Desjardins, C. Lavoie, *J. Appl. Phys.* **2011**, *110*, 113524.
[9] R. T. Tung, J. M. Gibson, J. M. Poate, *Phys. Rev. Lett.* **1983**, *50*, 429.
[10] X. Gao, J. Andersson, T. Kubart, T. Nyberg, U. Smith, J. Lu, L. Hultman, A. J. Kellock, Z. Zhang, C. Lavoie, S.-L. Zhang, *Electrochem. Solid-State Lett.* **2011**, *14*, H268.
[11] D. Zhang, J. Sheng, C. Zhao, J. Xu, J. Gao, S. Mao, Y. Men, P. Liu, J. Zhang, X. Luo, J. Li, W. Wang, D. Chen, T. Ye, J. Luo, *ECS J. Solid State Sci. Technol.* **2020**, *9*, 034001.
[12] T. T. Tran, C. Lavoie, Z. Zhang, D. Primetzhofer, *Appl. Surf. Sci.* **2021**, *536*, 147781.
[13] J. M. Gibson, J. L. Batstone, R. T. Tung, F. C. Unterwald, *Phys. Rev. Lett.* **1988**, *60*, 1158.
[14] P. A. Bennett, M. Y. Lee, P. Yang, R. Schuster, P. J. Eng, I. K. Robinson, *Phys. Rev. Lett.* **1995**, *75*, 2726.
[15] K. De Keyser, C. Van Bockstael, R. L. Van Meirhaeghe, C. Detavernier, E. Verleysen, H. Bender, W. Vandervorst, J. Jordan-Sweet, C. Lavoie, *Appl. Phys. Lett.* **2010**, *96*, 173503.
[16] I. Lindau, W. E. Spicer, *J. Electron Spectrosc. Relat. Phenom.* **1974**, *3*, 409.
[17] Z. Zhang, B. Yang, Y. Zhu, S. Gaudet, S. Rossnagel, A. J. Kellock, A. Ozcan, C. Murray, P. Desjardins, S.-L. Zhang, J. Jordan-Sweet, C. Lavoie, *Appl. Phys. Lett.* **2010**, *97*, 252108.
[18] R. A. Donaton, *Electrochem. Solid-State Lett.* **1999**, *2*, 195.
[19] M. Draxler, R. Beikler, E. Taglauer, K. Schmid, R. Gruber, S. N. Ermolov, P. Bauer, *Phys. Rev. A* **2003**, *68*, 022901.
[20] T. T. Tran, L. Jablonka, B. Bruckner, S. Rund, D. Roth, M. A. Sortica, P. Bauer, Z. Zhang, D. Primetzhofer, *Phys. Rev. A* **2019**, *100*, 032705.
[21] S. Gaudet, C. Coia, P. Desjardins, C. Lavoie, *J. Appl. Phys.* **2010**, *107*, 093515.
[22] T. T. Tran, L. Jablonka, C. Lavoie, Z. Zhang, D. Primetzhofer, *Sci. Rep.* **2020**, *10*, 10249.
[23] S.-L. Zhang, Z. Zhang, in *Metallic Films for Electronic, Optical and Magnetic Applications*, Elsevier, Amsterdam **2014**, pp. 244–301.
[24] L.-T. Zhao, M. Liu, Q.-H. Ren, C.-H. Liu, Q. Liu, L.-L. Chen, Y. Spiegel, F. Torregrosa, W. Yu, Q.-T. Zhao, *Nanotechnology* **2020**, *31*, 205201.
[25] K. van Stiphout, F. A. Geenen, N. M. Santos, S. M. C. Miranda, V. Joly, J. Demeulemeester, C. Mocuta, C. M. Comrie, C. Detavernier, L. M. C. Pereira, K. Temst, A. Vantomme, *J. Phys. D: Appl. Phys.* **2021**, *54*, 015307.
[26] M. Draxler, S. N. Markin, S. N. Ermolov, K. Schmid, C. Hesch, A. Poschacher, R. Gruber, M. Bergsmann, P. Bauer, *Vacuum* **2004**, *73*, 39.
[27] D. Primetzhofer, S. N. Markin, J. I. Juaristi, E. Taglauer, P. Bauer, *Phys. Rev. Lett.* **2008**, *100*, 213201.
[28] D. Primetzhofer, M. Spitz, S. N. Markin, E. Taglauer, P. Bauer, *Phys. Rev. B* **2009**, *80*, 125425.
[29] M. K. Linnarsson, A. Hallén, J. Åström, D. Primetzhofer, S. Legendre, G. Possnert, *Rev. Sci. Instrum.* **2012**, *83*, 095107.
[30] M. A. Sortica, M. K. Linnarsson, D. Wessman, S. Lohmann, D. Primetzhofer, *Nucl. Instrum. Methods Phys. Res., Sect. B* **2020**, *463*, 16.
[31] D. Primetzhofer, E. D. Litta, A. Hallén, M. K. Linnarsson, G. Possnert, *Nucl. Instrum. Methods Phys. Res., Sect. B* **2014**, *332*, 212.
[32] M. Mayer, in *AIP Conference Proceedings*, AIP, Denton, TX **1999**, pp. 541–544.

© 2022 The Authors. Small published by Wiley-VCH GmbH